



This is a repository copy of *Investigation of phase separation in InGaN alloys by plasmon loss spectroscopy in TEM.*

White Rose Research Online URL for this paper:  
<https://eprints.whiterose.ac.uk/187241/>

Version: Accepted Version

---

**Article:**

Wang, X., Chauvat, M.P., Ruterana, P. et al. (1 more author) (2016) Investigation of phase separation in InGaN alloys by plasmon loss spectroscopy in TEM. *MRS Advances*, 1 (40). pp. 2749-2756. ISSN 2059-8521

<https://doi.org/10.1557/adv.2016.542>

---

This is a post-peer-review, pre-copyedit version of an article published in *MRS Advances*. The final authenticated version is available online at:  
<http://dx.doi.org/10.1557/adv.2016.542>

**Reuse**

Items deposited in White Rose Research Online are protected by copyright, with all rights reserved unless indicated otherwise. They may be downloaded and/or printed for private study, or other acts as permitted by national copyright laws. The publisher or other rights holders may allow further reproduction and re-use of the full text version. This is indicated by the licence information on the White Rose Research Online record for the item.

**Takedown**

If you consider content in White Rose Research Online to be in breach of UK law, please notify us by emailing [eprints@whiterose.ac.uk](mailto:eprints@whiterose.ac.uk) including the URL of the record and the reason for the withdrawal request.



[eprints@whiterose.ac.uk](mailto:eprints@whiterose.ac.uk)  
<https://eprints.whiterose.ac.uk/>

# Investigation of phase separation in InGaN alloys by plasmon loss spectroscopy in a TEM

Xiaoyi Wang<sup>1</sup>, Marie-Pierre Chauvat<sup>2</sup>, Pierre Ruterana<sup>2</sup> and Thomas Walther<sup>1\*</sup>

<sup>1</sup> Dept. Electronic & Electrical Eng., University of Sheffield, Mappin St., Sheffield S1 3JD, UK

<sup>2</sup> CIMAP, UMR 6252, CNRS-ENSICAEN-CEA-UCBN, 14050 Caen, cedex, France

\*Email: [t.walther@sheffield.ac.uk](mailto:t.walther@sheffield.ac.uk)

## ABSTRACT

Phase separation of  $\text{In}_x\text{Ga}_{1-x}\text{N}$  alloys into Ga-rich and In-rich regions was observed by a number of research groups for samples grown with high indium content,  $x$ . Due to the radiation sensitivity of InGaN to beam damage by fast electrons, high-resolution imaging in transmission electron microscopy (TEM) or core-loss electron energy-loss spectroscopy (EELS) may lead to erroneous results. Low-loss EELS can yield spectra of the plasmon loss regions at much lower electron fluxes. Unfortunately, due to their delayed edge onset, the low energetic core losses of Ga and In partially overlap with the plasmon peaks, all of which shift with indium content.

Here we demonstrate a method to quantify phase separation in InGaN thin films from the low-loss region in EELS by simultaneously fitting both plasmon and core losses over the energy range of 13-30eV. Phase separation is shown to lead to a broadening of the plasmon peak and the overlapping core losses, resulting in an unreliable determination of the indium concentration from analyzing the plasmon peak position alone if phase separation is present. For  $x=0.3$  and  $x=0.59$ , the relative contributions of the binary compounds are negligibly small and indicate random alloys. For  $x_{\text{nom.}}=0.62$  we observed strong broadening, indicating phase separation.

## INTRODUCTION

Optoelectronic devices based on ternary InGaN alloys can cover a wide range of optical emission and absorption, from near ultraviolet (GaN) to infrared telecom wavelengths (InN). However, InGaN growth is a complex process and a number of phenomena such as ordering [1] crystallographic defects [2] as well as phase separation [3] may significantly influence the device performance [4-6]. Phase separation of  $\text{In}_x\text{Ga}_{1-x}\text{N}$  alloys into Ga-rich and In-rich regions was first predicted by Ho and Stringfellow [7] and later observed by a number of research groups. InGaN samples grown at high temperatures are particularly prone to this. As the indium concentration controls the optical emission properties of InGaN it is important to quantify any degree of phase separation in an InGaN thin film. However, due to the radiation sensitivity of InGaN to beam damage by fast electrons, as observed by O'Neill et al. [8] and Smeeton et al. [9], high electron fluxes as typically used in extended high-resolution imaging in transmission electron microscopy (TEM) or core-loss electron energy-loss spectroscopy (EELS) may lead to erroneous results.

Low-loss EELS can yield spectra of the plasmon loss regions at much lower electron fluxes and so potentially prevent or at least reduce beam damage in the TEM. Unfortunately, due to their delayed edge onset, the low energetic core losses of gallium (Ga 3d transitions yield  $M_{4,5}$  peaks at 23.8 and 28.5eV) and indium (In 4d transitions yield  $N_{4,5}$  peaks at 20.0 and 25.9eV) overlap with the plasmon peaks, which shift from 19.35eV for GaN to 15.5eV for InN.

Here we demonstrate a method to quantify phase separation in InGaN thin films by fitting both plasmon and core losses over the energy range of 13-30eV., especially for growth of high indium concentration InGaN, if high vapour pressure for the nitrogen precursor is applied [10]. Matsuoka et al. reported the growth of InGaN alloys by low temperature (500°C) metalorganic chemical vapour deposition (MOCVD) with In concentration up to 42%. Several studies indicated the growth of InGaN thin films and  $\text{In}_x\text{Ga}_{1-x}\text{N}/\text{In}_y\text{Ga}_{1-y}\text{N}$  heterostructures by MOCVD at temperatures in the range of 700°C-800°C may maximally achieve  $x=30\%$  of In content [11-14]. Previously, a quantification of the degree of phase separation was only possible by Rutherford backscattering spectrometry (RBS).

In this paper we report a method to quantify the degree of phase separation in InGaN thin film samples by applying multiple linear-least squares (MLLS) regression to InGaN valence electron energy loss spectra (VEELS).

## **EXPERIMENTAL**

### **Growth of InGaN samples**

The investigated InGaN samples were grown by metal organic vapour phase epitaxy (MOVPE) in a close couple shower head AIXTRON reactor using trimethyl-gallium (TEGa) and trimethyl-indium (TMIn) for the metals and  $\text{NH}_3$  for nitrogen. Three parameters have been investigated for the control of the indium incorporation: growth temperature, chamber pressure and III/V ratio. The growth of highest indium content layers has been carried out at the lowest temperature of 550°C, as well as highest III/V ratio (>40,000).

### **EELS characterization**

The EELS experiments were carried in a JEOL 2010F analytical TEM equipped with a Schottky field-emission gun, operated at 197kV (this voltage allows the user to increase the high tension by up to 3kV for energy-filtered imaging, cf. [15]). The microscope is equipped with a Gatan Imaging Filter (GIF 200) that allows for an energy resolution of  $\sim 0.9$  eV (FWHM of zero loss peak). The diffraction mode was applied to record EELS spectra with a collection semi-angle of  $\sim 20$  mrad. The dispersion of the spectrometer was measured as 0.0502eV per channel (calibrated by drift tube offsetting).  $\sim 5$ nA beam current and  $\sim 50$ nm probe size were set up to avoid electron beam-induced damage of the sample. Several spectra were recorded for each thin film sample, from different regions of different specimen thicknesses. The spectrometer dispersion was constant over the left half of the detector where zero loss peak and plasmon loss were located, as confirmed earlier by others [16]. Drift of the high tension or the magnetic prism strength is not a problem as the zero loss is recorded within all low loss spectra and it is only the distance of the plasmon peak from the zero loss peak that matters for this investigation.

## **RESULTS AND DISCUSSION**

For MLLS regression to fit experimental spectra of ternary InGaN, spectra of the binary compounds InN and GaN are used as references. Least-squares fitting of Lorentzian functions was used to model the smoothed plasmon loss spectra of InN and GaN, as shown in figure 1.

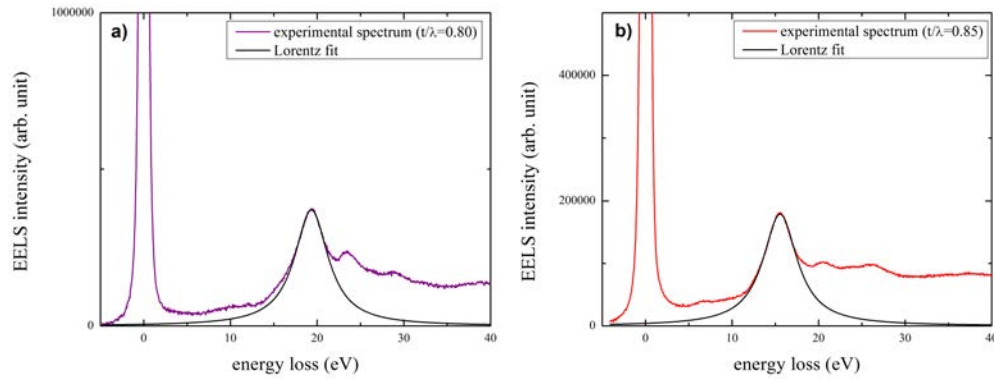


**Figure 1.** Lorentzian fits for GaN (a) and for InN (b) spectrum.

The selection of the reference spectra depends on the relative thicknesses of the measured regions. Ideally, a perfect reference spectrum should be measured from a region of relative thickness equal to the inelastic mean free path,  $\lambda$ , because for  $t/\lambda \sim 1$  the first plasmon intensity is maximal. The fitting window chosen for InN and GaN plasmon peaks was  $\pm 2$  eV wide, centered at the corresponding plasmon peak position, in order to reduce contribution from Cherenkov radiation and scattering in the low loss region (0-10eV), which would make the determination of the plasmon peak position less precise. Simultaneously, the full wide at half maximum (FWHM) of fitted plasmon losses can be evaluated and compared with spectra from ternary InGaN with different indium concentrations that have been fit in a similar way (figure 2).

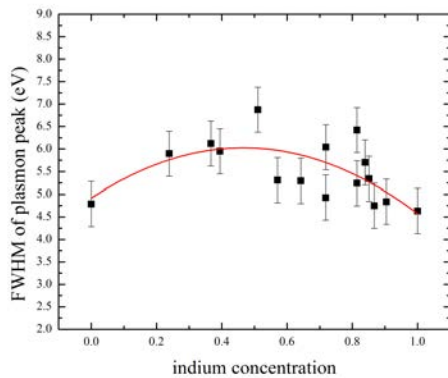


**Figure 2.** plot of FWHM of plasmon peak as function of indium concentration.

The experimental FWHM of the plasmon loss shows a parabolic characteristic across the range from  $x=0$  to  $x=1$ . The core-loss contribution to each spectrum is obtained by subtracting the fitted plasmon loss from the experimental spectrum. These artificial core-loss spectra for InGaN are then smoothed using a *Fast Fourier Transform* (FFT) method, in order to filter out the high frequency shot noise using a window 18 pixels wide (0.9 eV). The reconstructed core-loss spectra for GaN and InN are shown in figure 3. Note that the indium core loss peaks at  $\sim 20$ eV and  $\sim 26$ eV ( $N_{5,4}$ ) in figures 1, 3 and 5 are due to electronic  $4d \rightarrow 5p$  orbital transitions and much less well defined than the corresponding gallium  $M_{5,4}$  core loss peaks [17]. This is typical of N-edges and generally can make fitting for higher indium alloy concentrations (as in figure 7) more problematic despite reasonably high  $R^2$  values.

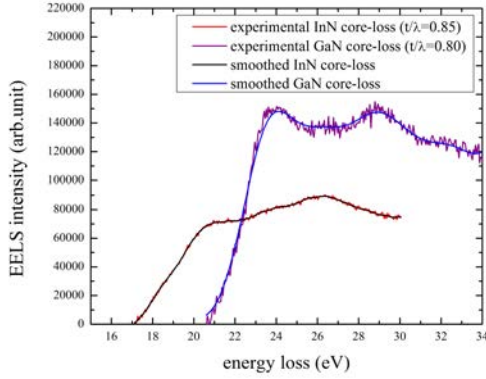


**Figure 3.** smoothed InN and GaN core-loss contributions after zero loss peak and plasmon subtraction

In order to synthesize the core-loss spectrum for a perfect InGaN alloy with indium content  $x$ , the GaN and InN core-loss spectra from different thicknesses and experimental intensities have been normalized with respect to relative thickness and total intensity according to equation 1:

$$S_{\text{normalized}} = S_{\text{core loss}} / [(t/\lambda) \int I_{\text{total}}(E) dE] \quad (1)$$

where  $S_{\text{core loss}}$  is the experimental core-loss spectrum profile,  $t/\lambda$  is the relative thickness of the specimen and  $\int I_{\text{total}}(E) dE$  is the integral of total EELS intensity of the spectrum.

To model the InGaN core-loss we superimpose the core-losses of GaN with weight  $(1-x)$  and of InN with weight  $x$ , where  $x$  is the indium concentration evaluated from the plasmon peak position [18], and we introduce an additional chemical shift of the synthesized core-loss contribution. The separation of core-loss and plasmon loss has been evaluated for the two binary and another two ternary alloy InGaN samples ( $x=0, 0.3, 0.86, 1$ ) that showed distinct plasmon peaks. The distance between the first core-loss and the plasmon peak position varied from 4.5 eV, increasing nonlinearly with the indium concentration (figure 4).

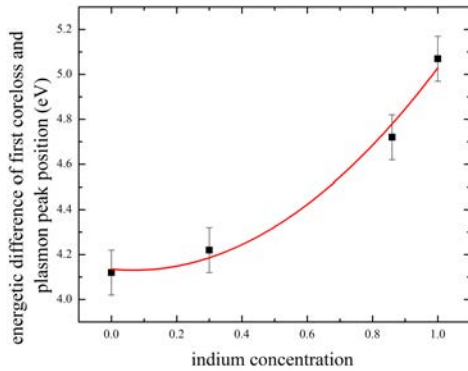


**Figure 4.** energetic difference measured between first core-losses (Ga  $M_5$ , In  $N_5$ ) and corresponding plasmon peak positions for different InGaN samples.

By applying second order polynomial fitting of the form  $a+bx+cx^2$ , the bowing parameter in figure 4 is determined as  $c=1.04 \pm 0.46$  eV. The bowing reflects the bandgap change with indium concentration, which follows Vegard's law with a bowing factor of 1.3-1.4eV for  $\text{In}_x\text{Ga}_{1-x}\text{N}$  [19]. The core-loss spectrum of  $\text{In}_x\text{Ga}_{1-x}\text{N}$  for a specific thickness  $t$  and a total integral spectral intensity is constructed from the normalized reference spectra by multiplication with a factor of

$(t/\lambda) \int I_{\text{total}}(E) dE$ . After combining the reference plasmon and core-loss spectra, the simulated spectra in the indium concentration range from 0 to 1 are depicted in figure 5.

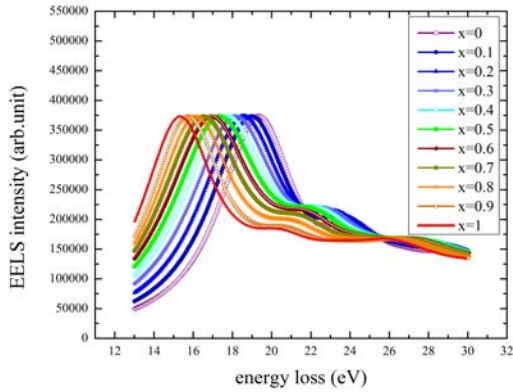


**Figure 5.** simulated InGaN reference spectra from  $x=0$  to  $x=1$ .

MLLS regression has then been applied to fit experimental EELS of  $\text{In}_{0.2}\text{Ga}_{0.8}\text{N}$ ,  $\text{In}_{0.3}\text{Ga}_{0.7}\text{N}$ ,  $\text{In}_{0.59}\text{Ga}_{0.41}\text{N}$  and  $\text{In}_{0.86}\text{Ga}_{0.14}\text{N}$  in the range of 13-30 eV. As depicted in figure 6 for  $x=0.3$ , the adjusted  $R^2$  for each fitted spectrum is always  $>0.998$ , which indicates good fitting.

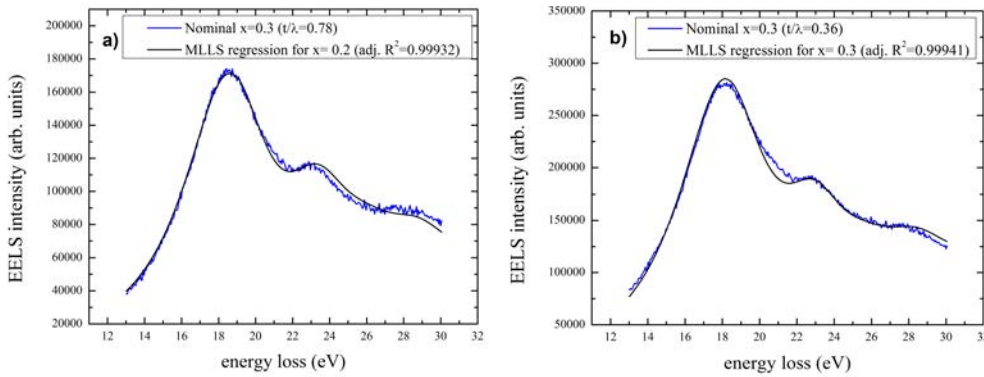


**Figure 6.** MLLS regression for  $\text{In}_{0.3}\text{Ga}_{0.7}\text{N}$ . Best fits are obtained for  $x=0.2$  (a) and  $x=0.3$  (b).

Some EELS spectra, presumably from phase separation regions, however, reveal much broader plasmon and core-losses without any clear peaks and cannot be fitted with one  $x$  value. We explain this as being due to additional contributions from InN and GaN. The indium concentrations determined from plasmon peak shift and weighted core-loss should be consistent. Additionally, the relative weightings ( $W$  in figure 7) for InGaN, GaN and InN calculated from plasmon and core-loss should also be consistent with the average value of  $x$ . MLLS regression was applied to fit EELS spectra from phase separated  $\text{In}_{0.59}\text{Ga}_{0.41}\text{N}$  (thin and thick) and  $\text{In}_{0.68}\text{Ga}_{0.32}\text{N}$  (figure 7), and the actual average indium content has been verified by EDXS [20].

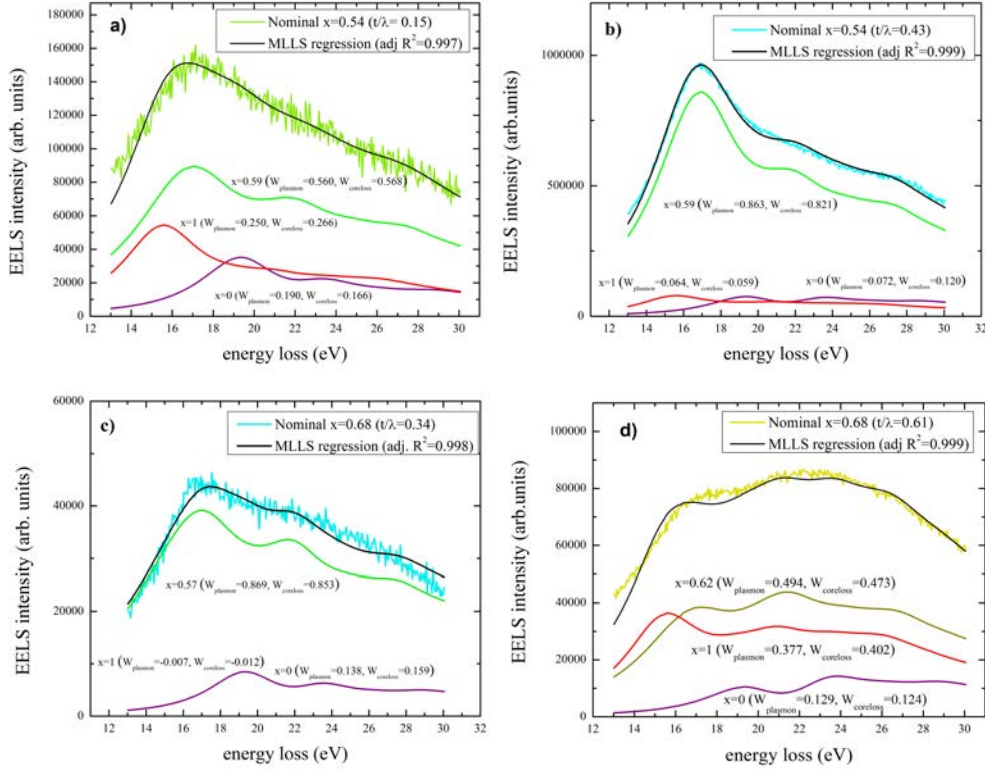


**Figure 7.** MLLS regression fits for a)  $\text{In}_{0.59}\text{Ga}_{0.41}\text{N}$  thin sample ( $t/\lambda=0.15$ , nominal:  $x=0.54$ , EDXS:  $x=0.59$ ), b)  $\text{In}_{0.59}\text{Ga}_{0.41}\text{N}$  thick sample ( $t/\lambda=0.43$  nominal:  $x=0.54$ , EDXS:  $x=0.59$ ), c)  $\text{In}_{0.68}\text{Ga}_{0.32}\text{N}$  ( $t/\lambda=0.34$  nominal:  $x=0.62$ , EDXS:  $x=0.68$ ), d)  $\text{In}_{0.68}\text{Ga}_{0.32}\text{N}$  ( $t/\lambda=0.61$  nominal:  $x=0.62$ , EDXS:  $x=0.68$ ).

In figure 7c) the negative weighting for InN is attributed to noise. The determination of the degree of phase separation is related to the relative weightings ( $W$ ) of GaN and InN, and the degree of phase separation ( $D$ ) is defined in equation 2:

$$D = W_{\text{GaN}} + W_{\text{InN}} \quad (2)$$

After considering InN and GaN plasmon and core-loss contribution to the MLLS regression, mean indium concentration and the degree of phase separation can be determined.

**Table I.** degree of phase separation and average indium concentration for  $\text{In}_{0.59}\text{Ga}_{0.41}\text{N}$  and  $\text{In}_{0.68}\text{Ga}_{0.32}\text{N}$  samples of different relative thicknesses and broadened peaks in EELS.

EDXS indium concentration (measured) [19]	degree of phase separation	average indium concentration from plasmon and core-loss
0.59 ( $t/\lambda=0.15$ )	$D_{\text{plasmon}}=44\%$ $D_{\text{core-loss}}=43.2\%$	$x_{\text{plasmon}}= 0.580$ $x_{\text{core-loss}}= 0.600$
0.59 ( $t/\lambda=0.43$ )	$D_{\text{plasmon}}=13.6\%$ $D_{\text{core-loss}}=17.9\%$	$x_{\text{plasmon}}= 0.574$ $x_{\text{core-loss}}= 0.543$
0.68 ( $t/\lambda=0.34$ )	$D_{\text{plasmon}}=13.1\%$ $D_{\text{core-loss}}=14.7\%$	$x_{\text{plasmon}}= 0.502$ $x_{\text{core-loss}}= 0.499$
0.68 ( $t/\lambda=0.61$ )	$D_{\text{plasmon}}=50.6\%$ $D_{\text{core-loss}}=52.6\%$	$x_{\text{plasmon}}= 0.684$ $x_{\text{core-loss}}= 0.696$

As shown in Table I, the determination of indium concentration from fitted plasmon loss and core-loss is consistent (within  $\Delta x = 1.7\%$  by using the standard deviation calculation from difference between plasmon and core-loss determined average indium). A comparison with previous energy dispersive X-ray (EDXS) quantification of the indium content [20], where the nominal  $\text{In}_{0.54}\text{Ga}_{0.46}\text{N}$  and  $\text{In}_{0.62}\text{Ga}_{0.38}\text{N}$  samples showed an average indium concentration of 0.59 and 0.64 respectively, is consistent. These results are in a good agreement with MLLS fitting of the EELS spectra, except for the 0.68 ( $t/\lambda = 0.34$ ) sample, where the discrepancy is slightly larger. The adjusted  $R^2$  shows the high quality of MLLS fitting.

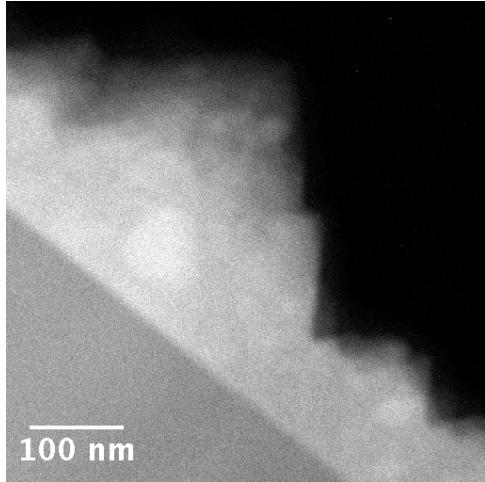


**Figure 8.** Annular dark field STEM image of islands in an  $\text{In}_{0.62}\text{Ga}_{0.38}\text{N}$  thin film sample where the brighter areas are supposed to be In richer.

While the initial experiments reported here have all been undertaken in a conventional Schottky field-emission transmission electron microscope (FEG-TEM), studies with aberration corrected instruments with their improved over-all stability of specimen stage and objective lens focus are now undertaken in STEM spectral imaging mode, where small electron beams can then be combined with longer acquisitions without drift.

## CONCLUSIONS

We have introduced a method to measure the degree of phase separation by using valence EELS. Our study confirmed that by applying MLLS regression to experimental spectra, one can determine the indium concentration and the degree of phase separation with high reliability (<2% difference from plasmon loss and core-loss fits).

## REFERENCES

1. P. Ruterana, G. Nouet, W. Van der Stricht, I Moerman and L. Considine, *Appl. Phys. Lett.* **72**, 1742 (1998).
2. D. Doppalapudia, S. N. Basu, K. F. Ludwig, Jr. and T. D. Moustakas, *J. Appl. Phys.* **84**, 1389(1998).

3. M. Zhu, S. You, T. Detchprohm, T. Paskova, E. A. Preble, D. Hanser and C. Wetzel, *Phys. Rev B* **81**, 125325 (2010).
4. P.II. Kyu, K.M. Ki, B.S. Ho, O.Y. Woo, S.T. Yeon, P.S. Ju, K.Y. Seok, M.Y. Tae and K.D. Joon, *Appl. Phys. Lett.* **87**, 061906 (2005).
5. L.Y. Sheng, M.K. Jeng, C. Hsu, S.W. Feng, Y.C. Cheng, C.C. Liao, C.C. Yang, C.C. Chou, C.M. Lee, and J.I. Chyi, *Appl. Phys. Lett.* **77**, 2988 (2000).
6. R. Singh, D. Doppalapudi, T.D. Moustakas and L.T. Romano, *Appl. Phys. Lett.* **70**, 1089 (1997).
7. I. Ho and G.B. Stringfellow, *Appl. Phys. Lett.* **69**, 2701 (1996).
8. J.P. O'Neill, I.M. Ross, A.G. Cullis, T. Wang and P.J. Parbrook, *Appl. Phys. Lett.* **83**, 1965 (2003).
9. T.M. Smeeton, M.J. Kappers, J.S. Barnard, M.E. Vickers and C.J. Humphreys, *Appl. Phys. Lett.* **83**, 5419 (2003).
10. T. Matsuoka, T. Sasaki and A. Katsui, *Optoelectronics* **5**, 53 (1990).
11. T. Matsuoka, N. Yoshimoto, T. Sasaki and A. Katsui, *J. Electron. Mater.* **21**, 157 (1992).
12. S. Nakamura, *Microelectron. J.* **25**, 651 (1994).
13. M. Shimizu, K. Hiramatsu and N. Sawaki, *J. Cryst. Growth.* **145**, 209 (1994).
14. S. Nakamura, T. Mukai, M. Senoh, S. Nagahama and N. Iwasa, *J. Appl. Phys.* **74**, 3911 (1993).
15. T. Walther, F. Wolf, A. Recnik and W. Mader, *Int. J. Mater. Res.* **97**, 934 (2006).
16. P.L. Potapov and D. Schryvers, *Ultramicroscopy* **99**, 73 (2004).
17. K.A. Mkhoyan, J. Silcox, E.S. Alldredge, N.W. Ashcroft, H. Lu, W.J. Schaff and L.F. Eastman, *Appl. Phys. Lett.* **82**, 1407 (2003).
18. X. Wang, M.P. Chauvat, P. Ruterana and T. Walther, *Semicond. Sci. Technol.* **30** (11), 114011 (2015).
19. R.R. Pelá, C. Caetano, M. Marques, L.G. Ferreira, J. Furthmüller and L.K. Teles, *J. Appl. Phys.* **98**, 151907 (2011).
20. T. Walther and X. Wang, *J. Microsc.* **252** (2), 151 (2015). doi: 10.1111/jmi.12291